NANO MICRO small

Supporting Information

for *Small,* DOI: 10.1002/smll.202102807

Targeted Nanoscale 3D Thermal Imaging of Tumor Cell Surface with Functionalized Quantum Dots

Jun Yang, Hanliang Du, Zhenhao Chai, Zheng Ling, Ben Q. Li, and Xuesong Mei*

Supplementary Information for

Targeted Nanoscale 3D Thermal Imaging of Tumor Cell Surface with Functionalized Quantum Dots

Jun Yang, Hanliang Du, Zhenhao Chai, Zheng Ling, Ben Q. Li, Xuesong Mei*

Dr.J.Yang, H.L.Du, Z.H.Chai, Z.Ling, Prof.X.S.Mei
State Key Laboratory for Manufacturing Systems Engineering, Xi'an Jiaotong University, Xi'an, 710049, China
Shaanxi Key Laboratory of Intelligent Robots, Xi'an Jiaotong University, Xi'an, 710049, China
E-mail: softyj@xjtu.edu.cn
Prof.B.Q.Li
Department of Mechanical Engineering, College of Engineering and Computer Science, University of Michigan, MI 48128, USA

1. Photothermal properties of quantum dots

Existing theoretical studies have shown that the peak wavelength of CdTe quantum dots synthesized in water phase has a good linear relationship with temperature in the range of 60℃ [1].

The theoretical analysis of linear photothermal properties of quantum dots can refer to the previous results of our team [2]. And the theoretical derivation process in this study is as follows:

The energy gap in a semiconductor quantum dot is related to the bulk semiconductor energy gap and the effect of quantum confinement,

$$E_g^{QD} = E_g + E^{conf} + E_{e-h} + J_{e-ph} \tag{S1}$$

where E_g^{QD} stands for the band gap of the QDs, E_g is the energy gap of the bulk semiconductor, E_{conf} is the quantum-confined energy, E_{e-h} is the electron–hole coulomb interaction energy, and J_{e-ph} is the electron–phonon coupling energy. Taking the derivative with respect to T, one has the result:

$$\frac{dE_g^{QD}}{dT} = \frac{dE_g}{dT} + \frac{dE^{conf}}{dT} + \frac{dE_{e-h}}{dT} + \frac{dJ_{e-ph}}{dT} \tag{S2}$$

For II–VI of the semiconductor QDs, analysis shows that lattice properties of these QDs resemble those of the bulk materials, even though the optical properties are quite distinct. Consequently, the temperature coefficient of $\frac{dE_g^{QD}}{dT}$ is similarly equivalent to the value of the corresponding bulk materials. The electron–phonon interaction term is rather small and thus can be neglected, and the E_{conf} and $E_{\text{e–h}}$ terms are also relatively insensitive to the temperature change.

A well-known relationship for the temperature dependent energy gap of the bulk semiconductor is expressed by the Varshni equation:

$$E_g = E_0 - \alpha \frac{T^2}{T + \beta} \tag{S3}$$

where E_0 represents the band gap of the bulk semiconductor at 0K, α is the temperature constant, and β is the approximate Debye temperature of the material. The band gap energy of QDs is equal to the energy of the emitted photon,

$$E_g^{QD} = \frac{\hbar c}{\lambda_{abs}} \tag{S4}$$

where $\hbar$ and c are Plank's constant and the velocity of light, respectively, and λ_{abs} is the wavelength of first excitonic absorption peak. With **Equation (S3)** substituted into **(S4)**, one has the following relation,

$$\frac{dE_g^{QD}}{dT} = -\frac{1239.84}{\lambda^2} \frac{d\lambda_{abs}}{dT} \tag{S5}$$

The temperature-induced band gap change can be expressed by the temperature dependent change of the first excitonic absorption peak wavelength. Due to the fact that the change of the first excitonic absorption peak wavelength $\frac{d\lambda_{abs}}{dT}$ is equal to the temperature-dependent change of the PL wavelength $\frac{d\lambda_{PL}}{dT}$ combining **Equation (S3)** and **(S5)** gives the thermo-spectral sensibility relation,

$$\lambda_{PL} = \frac{\lambda\lambda_0\alpha}{1239.84}T + \lambda_0\left[1 - \frac{\lambda\alpha\beta^2}{1239.84}\frac{T - T_0}{(T+\beta)(T_0+\beta)}\right] \quad \text{(S6)}$$

Making use of the fact that λ_{PL} is very close to λ_0, the above relation can be further approximated by a linear relation,

$$\lambda_{PL} = a + bT \quad \text{(S7)}$$

Actually, only a limited number of temperature values and peak wavelength values can be measured by experiments, and then the coefficient of the function can be identified by mathematical calculation, so that the function mapping of temperature to peak wavelength can be established. In this way, the temperature of the quantum dots to be measured can be deduced by measuring the relationship between the peak wavelength of a finite number of quantum dots and their temperature (**Figure 5** and **Equation (1)**).

The photo thermal characteristic calibration equipment of the functional quantum dot probe is shown in **Figure S1**.

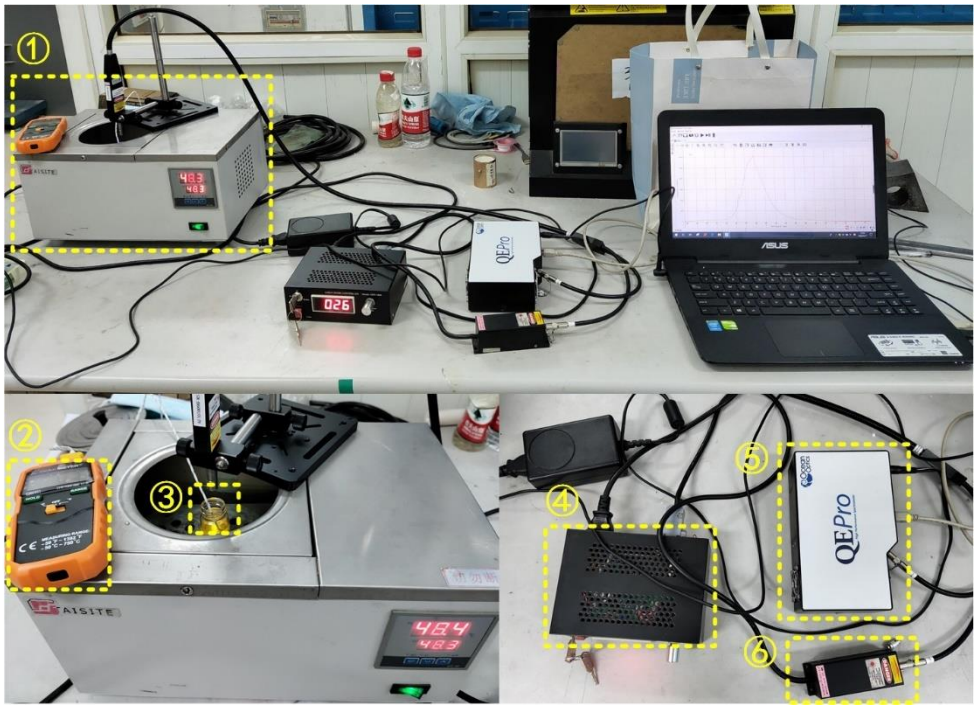

Figure S1. Fluorescence spectrum calibration equipment. 1) Water bath heating device; 2) Thermocouple; 3) Tf-QDs solution; 4) Laser controller; 5) Spectrometer; 6) Laser.

2. Tumor cell culture and targeted labeling experiment

Human osteosarcoma cells (HOS) cells were cultured in DMEM supplemented with 10% fetal bovine serum (FBS) and 1% double anti-tumor solution at 37℃ under 5% CO_2 for about 2-3 days. Once the cells were suitably confluent (70%-80%), 1 mL cell suspension with 1×10^5 cells was sub-cultured in a 20 mm confocal Petri dish, followed by incubation for a period of 10 h.

In the tumor cell targeted labeling experiment, the imaging of the tumor cells added with Tf-QDs solution and with non-functionalized QD solution are shown in **Figure S2**. The concentration of both probes was 0.5 μM. Compared with the functionalized Tf-QD probes, the non-functionalized QDs can not label the tumor cells effectively (the tumor cells with non-functionalized QDs have no fluorescence phenomenon in the dark field).

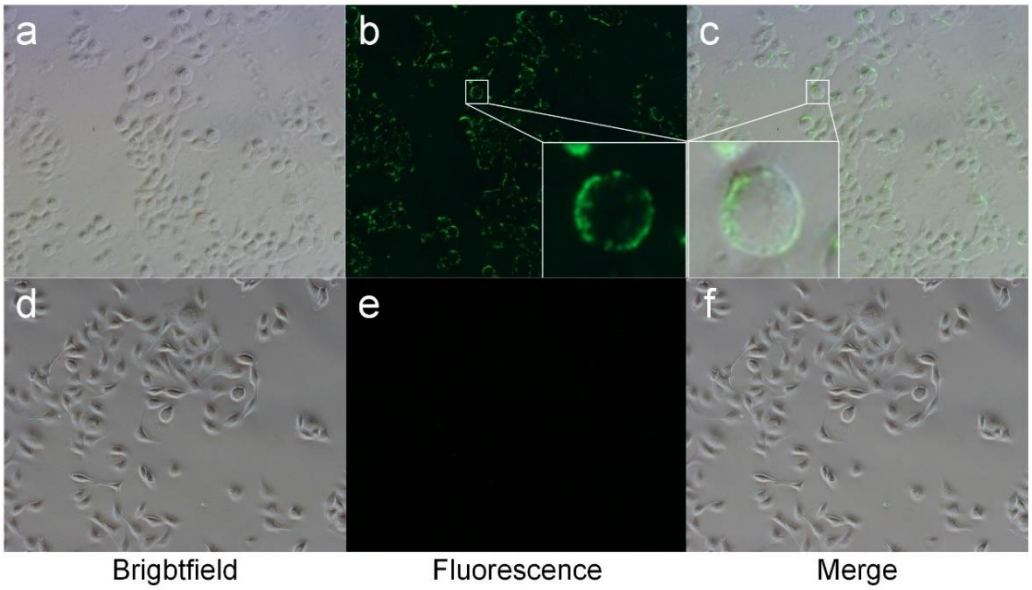

Figure S2. Representative images showing tumor cells labeled with (a, b, c) Tf-QDs and (d, e, f) non-functionalized QDs. (a, d) Bright field images, (b, e) fluorescence images, and (c, f) synthetic images.

3. Design and construction of nanoscale 3D thermal imaging system

The three-dimensional nanoscale tumor cell thermal imaging system is shown in **Figure 7**, and has been divided into three parts based on their functions: 1) fluorescence excitation and intracellular imaging of the QDs, 2) measurement of the

fluorescence spectra of the probes in the field of vision, and 3) modulation of the probe spot into a double helix spot to obtain the spatial position of the probe (**Figure S3**).

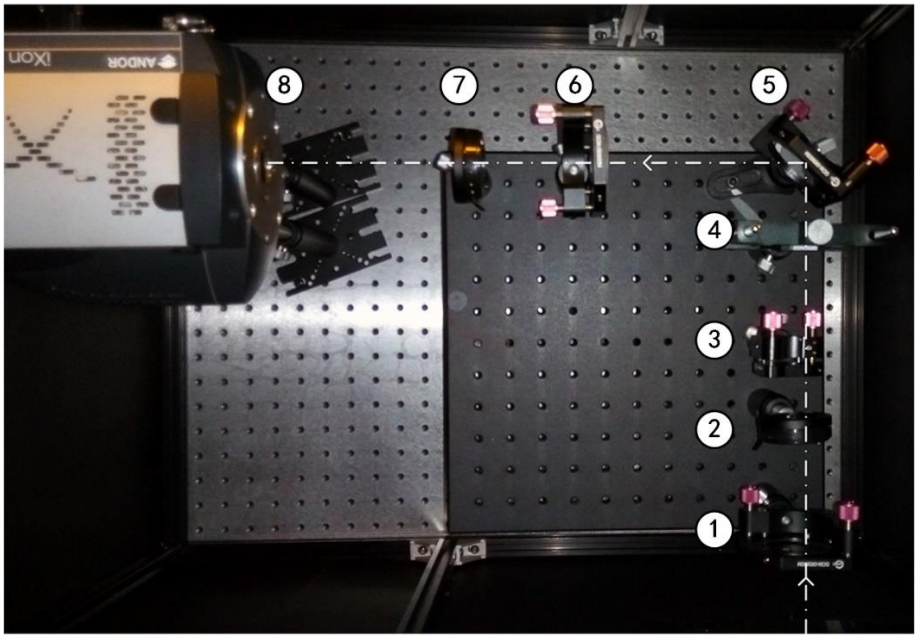

Figure S3. DH-PSF three-dimensional positioning imaging optical path. 1) lens; 2) diaphragm; 3) filter; 4) phase plate; 5) mirror; 6) lens; 7) diaphragm; 8) EMCCD.

4. Calibration of nanoscale 3D thermal imaging system

The theoretical analysis of the relationship between the rotation angle and the defocus distance in the DH-PSF imaging can be seen in our previous work [3]. In the process of double helix beam propagation, for any propagation plane, the maximum intensity point satisfies the condition $\theta=\dfrac{\Delta n_{jp}\tan^{-1}\dfrac{z_1}{z_R}+\phi_{jp}+2N\pi}{\Delta m_{jp}}(N=0,1,2,...)$. For two points $P_1(r_1, \theta_1, z_1)$ and $P_2(r_2, \theta_2, z_2)$ in space, assuming that they are not in the same propagation plane and have the largest light intensity in their respective planes, the angle between them is $\Delta\theta=\theta_1-\theta_2=\dfrac{\Delta n_{jp}}{\Delta m_{jp}}\left(\tan^{-1}\dfrac{z_1}{z_R}-\tan^{-1}\dfrac{z_2}{z_R}\right)+\dfrac{2\Delta N\pi}{\Delta m_{jp}}$. When $-\dfrac{\pi}{4}<\theta_1<\dfrac{\pi}{4}$ and point P_2 is in the focal plane, the relation between the angle ($\Delta\theta$)

between the two points and the distance (Δz) can be approximated as a linear relation. This is also the theoretical basis for fitting the rotation angle and defocus distance into a linear equation after calibration.

The lateral resolution of 3D thermal imaging system was calibrated by micrometer, and the axial resolution was calibrated by piezo nano-positioning stage. As shown in **Figure 8**, the relationship between the actual axial position of the imaging point and the rotation angle of the defocusing double helix spot is $\theta = -0.6026\Delta z$. The Z-axis axial positioning range of the system for a single imaging is about 2.6μm (-1.5μm ~ +1.1μm), and since the size of the camera's photosensitive element limits the single imaging field of view to 133μm×133μm, the three-dimensional positioning range of a single imaging of the system is 133μm×133μm×2.6μm. In addition, the calibration results show that the lateral positioning resolution ratio of the system in the XY plane is 128 nm, and the axial positioning resolution ratio of Z-axis is 138 nm.

5. Double helix spot image processing method

As the shape of the double helix spot is irregular, image processing is needed to determine the rotation angle. And in order to determine the rotation angle, the center positions of the two light spots have to be identified.

The interference of ambient light and other nontarget probe fluorescence exists in the actual optical imaging. In the obtained double spot image, the shape of a single spot is not an ideal ellipse, but has a certain dispersion distribution range. And due to the existence of noise points and interference peaks, the actual spot distribution is irregular.

In this paper, the centroid method is used to recognize the center of double spot image. The process of spot center recognition is as follows: firstly, the contrast of the image is enhanced, then the image is binarized, and the edge of the spot is smoothed by morphological opening, and then the centroid method is used to identify the spot center. Among them, contrast enhancement, binarization and morphological opening are all basic image processing operations, which have been used and verified in many

existing literatures.

The centroid method is the key point of this paper. According to the existing research [4], centroid method is a common and widely applicable method in the field of spot center positioning. The centroid method is sufficient to ensure the accuracy of spot center recognition in this paper because the number of target probes detected in this paper is not large and the distribution is not dense.

Image processing and spot center recognition as shown in **Figure S4** (with probe 1 as an example).

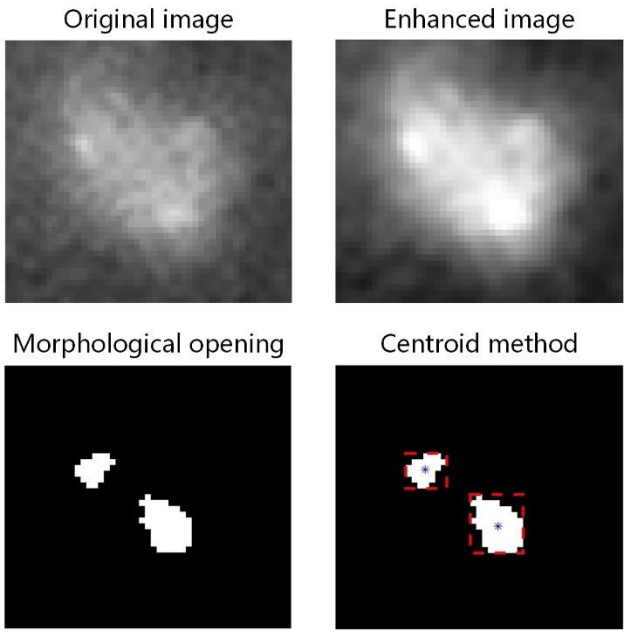

Figure S4. Image processing and spot center identification

After extracting the center position of the light spot in the image, the angle between the line connecting the two light spot centers and the horizontal line is further calculated, which is the rotation angle θ of the double helix spot image (**Figure S5**).

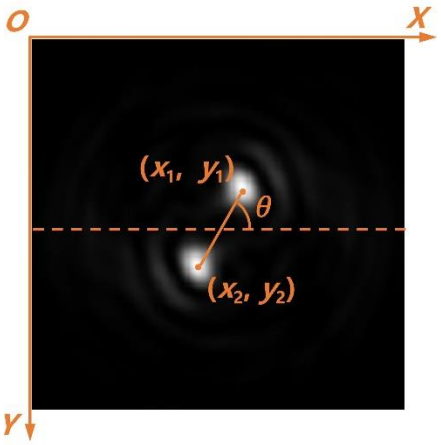

Figure S5. The rotation angle θ of the double helix spot image

References

[1] Jiang, X.; Shao, J.; Li, B. Q., *Appl. Surf. Sci.* **2017,** *394*, 554.

[2] Jiang, X.; Li, B. Q.; Qu, X.; Yang, H.; Liu, H., *Journal of Materials Chemistry B* **2017,** *5*, 8983.

[3] Yang, J.; Ling, Z.; Li, R.; Mei, X., *Journal of Physics D-Applied Physics* **2019,** *52*, 365401.

[4] Parthasarathy, R., *Nature Methods* **2012,** 9, 724.